metals

MDPI

Article

Porous Titanium Surfaces to Control Bacteria Growth: Mechanical Properties and Sulfonated Polyetheretherketone Coatings as Antibiofouling Approaches

Ana M. Beltrán [1,*], Ana Civantos [2], Cristina Dominguez-Trujillo [1], Rocío Moriche [1], José A. Rodríguez-Ortiz [1], Francisco García-Moreno [3], Thomas J. Webster [4], Paul H. Kamm [3], Andrea Mesa Restrepo [2] and Yadir Torres [1,*]

1 Departamento de Ingeniería y Ciencia de los Materiales y del Transporte, Escuela Politécnica Superior, Universidad de Sevilla, Virgen de África 7, 41011 Sevilla, Espana
2 Micro and Nanotechnology Laboratory, University of Illinois at Urbana-Champaign, 208 N Wright St, Urbana, IL 61801, USA
3 Institute of Applied Materials, Helmholtz-Zentrum Berlin für Materialien und Energie, Hahn-Meitner-Platz 1, 14109 Berlin, Germany
4 Department of Chemical Engineering, Northeastern University, Boston, MA 02115, USA
* Correspondence: abeltran3@us.es (A.M.B.); ytorres@us.es (Y.T.)

Received: 19 July 2019; Accepted: 5 September 2019; Published: 10 September 2019

Abstract: Here, titanium porous substrates were fabricated by a space holder technique. The relationship between microstructural characteristics (pore equivalent diameter, mean free-path between pores, roughness and contact surface), mechanical properties (Young's modulus, yield strength and dynamic micro-hardness) and bacterial behavior are discussed. The bacterial strains evaluated are often found on dental implants: Methicillin-resistant *Staphylococcus aureus* (MRSA) and *Pseudomonas aeruginosa*. The colony-forming units increased with the size of the spacer for both types of studied strains. An antibiofouling synthetic coating based on a sulfonated polyetheretherketone polymer revealed an effective chemical surface modification for inhibiting MRSA adhesion and growth. These findings collectively suggest that porous titanium implants designed with a pore size of 100–200 μm can be considered most suitable, assuring the best biomechanical and bifunctional anti-bacterial properties.

Keywords: porous commercially pure titanium; osseointegration; sulfonated PEEK polymer; instrumented micro indentation; bacterial behavior

1. Introduction

Bacterial infection of medical devices is one of the most common causes of implant failure. Device-associated infections are crucial health issues and usually occur during the first two years after surgery. More than 60–70% of total hip replacements and knee arthroplasties are infected during this time [1]. In the dental industry, peri-implantitis is considered the most frequent inflammatory process related to infected dental implants in which bacteria can attach and colonize the area around the implants and the inner titanium (Ti) surfaces, affecting both soft and hard tissue [2]. In the last few decades, the frequency of peri-implantitis has increased from 14% to 30% [3], becoming a high-risk factor for patient health which harnesses the performance of implants. Attached bacteria can grow fast and develop a biofilm as part of normal bacteria behavior, which can be in a hospital environment, on the surface of medical implants, and/or on instruments during surgery. The main function of these

biofilms is to protect bacteria and promote their spreading to other areas in which they will form a biofilm. Two important features of this biofilm are its resistance to antibiotics and its ability to keep bacteria hidden from the immune system [4].

A broad spectrum of bacteria is presented in the buccal cavity around the implant and even in daily environments such us food, drinking water and medical supplies [5,6]. Among them, *Porphyromonas gingivalis*, *Pseudomonas aeruginosa* (PA), *Fusobacterium nucleatum*, and Methicillin-resistant *Staphylococcus aureus* (MRSA) are the main strains that commonly cause bacterial infections in implantology [7]. MRSA is a Gram-positive bacterium which has increased resistance to main antibiotic treatments [8,9] while *P. aeruginosa* is a Gram-negative bacterium that can easily develop a fast biofilm [10,11].

On the other hand, there are other common factors that limit and reduce the osseointegration of dental implants related to their mechanical properties. Commercially pure titanium (c.p. Ti) is frequently used as a biomaterial in the orthopedic and dental industries. Indeed, most metallic screws used are medical grade IV and are fabricated using pure titanium [12]. Regarding the stiffness of this type of pure titanium, the Young´s modulus (E) values are higher than those reported for cortical bone (100–110 vs. 20–25 GPa, respectively). This significant difference in Young's modulus can lead to the stress-shielding phenomenon [13], which can impair dental implant fixation. Several studies have focused on alternatives to reduce this stress-shielding effect by designing porous substrates with a similar Young´s modulus to bone tissue [14–16]. Therefore, the development of porous materials is an attractive and effective approach to fabricate clinical devices with improved osseointegration properties [16–18].

However, surface roughness, the presence of pores, and the joining of typical metallic implants can favor the adhesion and proliferation of bacteria, with a consequent risk of infections for the patient. In addition, the role of the surface chemistry in the evolution of these infections needs to be considered with implant failures. Antibiotic treatment, based on the administration of gentamicin, cefazolin, and vancomycin [19] alone or in combination, is more effective for planktonic bacteria compared to bacteria in a biofilm [20]. After biofilm formation, a higher antibiotic dosage—associated with higher tissue toxicity—and even longer administration periods are needed but are not always successful for killing bacteria. Indeed, both strategies potentiate the development of bacteria resistance, reducing the effectiveness of these pharmaceutical strategies. Some studies have shown that the amount of antibiotic needed to effectively kill bacteria protected by a biofilm is 10–1000 times [20,21] higher compared to the dosage applied for the same strain planktonic bacteria.

Other alternatives have been proposed to reduce bacterial infection not only by killing them by using bactericidal substances such as silver [22–24], gold, copper, magnesium, and TiO_2 (among others) [25] nanoparticles but also by inhibiting their adhesion process by using antibiofouling substrates. Unfortunately, none of these approaches have been truly effective, and there are still some safety concerns related to nanoparticle-controlled release in medicine. The antibacterial properties observed on TiO_2 films should be mentioned. Several authors have developed TiO_2 films onto different substrates (such as polyethylene) using radio frequency plasma (RF plasma) or activated by ultraviolet light in the C-spectra region (UVC) to understand the chemical shifts that reduce or kill bacteria [26,27]. In these studies, a relationship between a homogeneous TiO_2 film with its particle size, Ti-ionic species, crystal structure and antibiofouling properties against *Escherichia coli* (E. coli) has been found. However, the effect of topographical changes, such as roughness and porosity parameters, has not been evaluated; thus, further research should be performed.

For those reasons, the latest advances in antibacterial treatments have focused on surface passivation and designing antibiofouling and bactericidal surfaces which can potentially reduce or even kill the bacteria attached in order to avoid biofilm formation and later colonization [26–29]. In this context, several strategies have been developed to create effective inorganic and organic coatings with antibacterial properties such as metals and nitric oxides, ceramics, carbon-based coatings, polyetheretherketone (PEEK), and chitosan, or with anti-bacterial nanoparticles [30–32]. Particularly, PEEK presents good biocompatibility and a lower Young's modulus more similar to bone tissue that

can be easily modified to generate coatings for reinforced titanium with carbon nanotubes [33] or combined with other elements [34,35].

Hence, in this work, we have developed porous c.p. Ti substrates to correlate surface and mechanical properties that affect the adhesion of MRSA and *P. aeruginosa* bacteria, including a chemical modification using sulfonated PEEK (termed SPEEK) as a coating on these porous substrates. The microstructure of porous c.p. Ti fabricated using the space-holder technique was analyzed in terms of macro- and micro-mechanical properties (*P-h* curves and pseudo-creep effects) as well as for bacterial behavior depending on the pore size, roughness and SPEEK coating modifications. Results were compared to a fully-dense c.p. Ti substrate.

2. Materials and Methods

Figure 1 summarizes the experimental protocols used to fabricate and characterize fully-dense and porous substrates followed by the SPEEK coating onto porous substrates. Then, the porosity features and their influence on the mechanical and bacterial behavior of fully dense and porous specimens were evaluated. Finally, the role of the SPEEK coating is analyzed in terms of bacteria behavior.

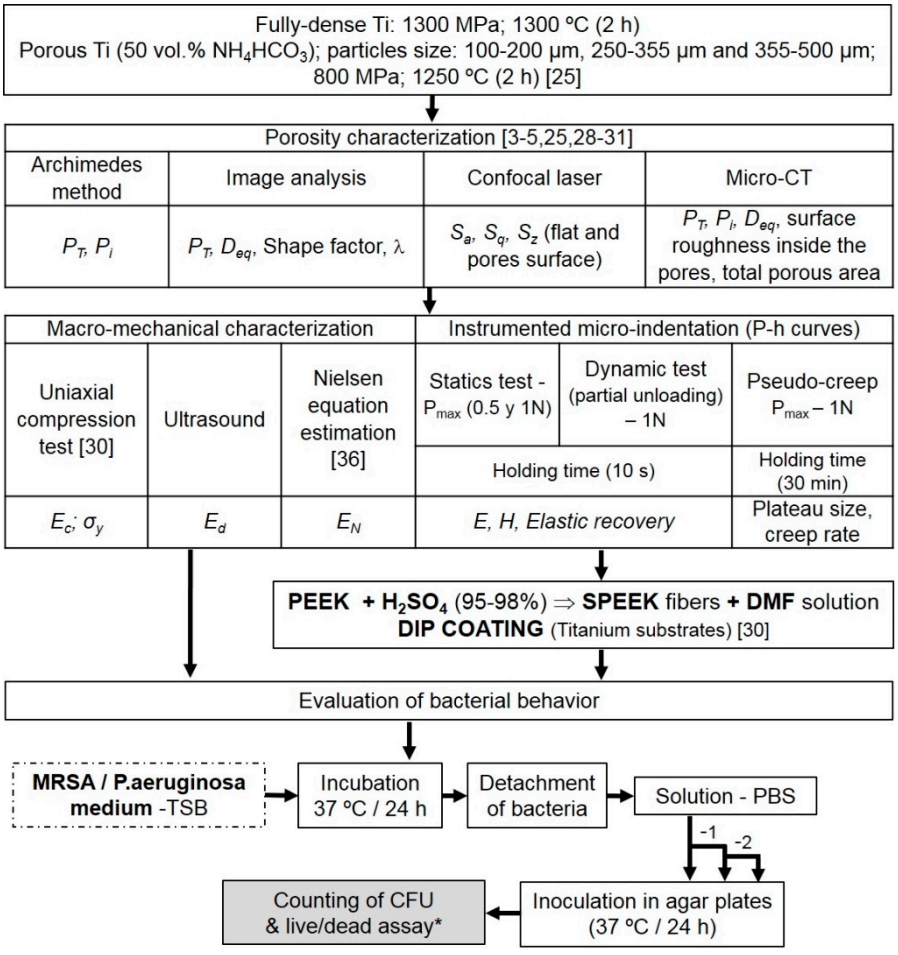

Figure 1. Diagram showing the fabrication, characterization and bacteria designed experiments of uncoated and coated with sulfonated polyetheretherketone (SPEEK) on porous commercially pure titanium (c.p. Ti) substrates. * Note: A live–dead assay was only performed on the studies with methicillin-resistant *Staphylococcus aureus* (MRSA).

2.1. Fabrication of Fully-Dense and Porous Titanium Substrates

Fully-dense c.p. Ti samples were obtained by conventional powder-metallurgy technology (PM), while porous substrates were fabricated using the space-holder technique (SHT) with 50 vol. %

and three different particle size ranges of NH_4HCO_3 particles—100–200, 250–355 and 355–500 μm (see Figure 1). The powder-metallurgy technique, the ranges of pore sizes, and the percentage of the space holder were thoroughly studied before by our research group regarding their mechanical properties related to the porosity index and their relationship with osteoblastic and immune cell behavior [14–16,18,36–40]. Briefly, c.p. Ti powder produced by a hydrogenation/dehydrogenation process was used as the starting powder (SE-JONG Materials Co. Ltd., Incheon, Korea). The chemical composition of the c.p. Ti powder was equivalent to c.p. Ti Grade IV (ASTM F67 00). The compacting pressures were 1300 MPa for the fully-dense substrate and 800 MPa for the porous substrates using an Instron 5505 universal testing machine (Instron, Reino Unido). Afterwards, spacer particles were thermally removed to obtain porous substrates. Finally, all of them were sintered in a ceramic tubular furnace at 1250 °C under a high vacuum. Later, the substrates were carefully grinded and polished to preserve their porosity fraction as well as size and morphology of the pores.

2.2. Fabrication and Deposition of the SPEEK Coating

Additionally, some of these substrates were also coated with SPEEK to evaluate its effect on the adhesion and proliferation of bacteria. The coating was prepared by dissolving 1 g of polyetheretherketone (PEEK; Sigma Aldrich, Barcelona, Spain) in 25 mL of concentrated sulfuric acid (H_2SO_4 at 95–98%, Sigma Aldrich) at 300 rpm for 4 h. This solution was decanted under a continuous mechanical agitation sulfonating reaction, and, after that, it was washed until it reached a neutral pH. Finally, SPEEK was dried under vacuum conditions for 24 h followed by another 24 h in a furnace at 65 °C. The dried fibers were dissolved in a dimethylformamide (DMF) solution at 4 wt. % to prepare the coating solution [39]. The coating process was carried out by dipping the porous and fully-dense c.p. Ti substrates into the prepared SPEEK solution. The immersion speed was controlled to generate a uniform surface coating (about 5 mm/min). However, the adhesion of the coating depends on the contact angle of the surfaces, which is particularly critical for fully-dense samples. After the immersion, the coated samples were dried in an oven for 4 h at 250 °C.

2.3. Microstructural and Mechanical Characterization of the c.p. Ti Substrates

The microstructural parameters and surface roughness of both the fully-dense and porous substrates were evaluated by different bi-dimensional (2D) and three dimensional (3D) techniques. The pores (total and interconnected fraction, equivalent diameter, shape factor, and mean free-path between pores) were studied using different techniques: Archimedes' method, image analysis (IA) and scanning electron microscopy (SEM). Furthermore, compositional analyses were performed on the SEM microscope (JEOL 6460LV, Japan) by energy dispersive spectroscopy (EDS). A confocal laser was used to evaluate surface roughness (at the flat area and inside the pores), arithmetical mean deviation (S_a), root mean square height (S_q) and maximum height (S_z). On the other hand, X-ray micro-computed tomography (M-CT) was performed due to its potential to provide 3D information of the surface roughness inside the pores, the total porous area, and the total surface area (flat surface + area inside the pores). Technical details about these characterization protocols have been already described by the authors in earlier work [14–16,18,36–39].

Uniaxial compression tests were performed to analyze the macro-mechanical behavior of the substrates following standard procedures [41]. A strain rate of 0.005 mm/mm·min was applied. All tests finished with a strain of 50%, and, afterward, the Young's modulus (E_c) and yield strength (σ_y) were determined considering the effect of the testing machine stiffness (87.9 kN/mm). Instrumented micro-indentation tests (*P-h* curves) were also used to evaluate the micro mechanical behavior of the porous substrates. Results were compared to those obtained for fully-dense c.p. Ti substrates. In this context, measurements were performed at different applied loads, different dwell times and methodologies for applying the load. All tests were carried out in a Microtest machine (MTR3/50-50/NI, Microtest S.L., Madrid, Spain) with a Vickers indenter. On porous c.p. Ti substrates, measurements were performed on representative areas which corresponded to the mean free path (λ) between pores

previously calculated by IA. Loading and unloading tests were carried out up to the largest load of 0.5 and 1 N with a load rate of 0.5 N/min, holding the load for 10 s. Additionally, quasistatic partial loading–unloading curves (dynamic tests) were performed up to a peak load of 1 N. Finally, we also evaluated the effect of the size of the residual Ti matrix between pores in a potential pseudo-creep behavior (at a holding time of 30 min under load control). At least three tests were performed for each substrate and test condition. The micro-hardness and elastic modulus were calculated using the Oliver and Pharr method [42], and corrections were made considering changes induced to the indenter geometry due to wear or damage from use. Micro-hardness was calculated from Equation (1) [42].

$$H = \frac{P_{max}}{A} \tag{1}$$

where P_{max} is the maximum load and A is the contact area, considering the depth of contact between the indenter and the sample surface, h_c. The effective elastic modulus (E_{eff}), which includes elastic displacements in both the indenter and the sample was calculated following Equation (2):

$$E_{eff} = \frac{S}{\beta \frac{2}{\sqrt{\pi}} \sqrt{A}} \tag{2}$$

where S is the slope of the unloading P-h curve and β is a correction factor, which is dependent on the indenter. The elastic modulus of the sample was then calculated from E_{eff} considering the elastic modulus (E_i) and the Poisson's ratio of the indenter (ν_i) and the material that we measured, in our case, c.p. Ti. (ν), following Equation (3):

$$E = \frac{\left(1 - \nu^2\right)}{\frac{1}{E_{eff}} - \frac{(1-\nu_i{}^2)}{E_i}} \tag{3}$$

2.4. Evaluation of Bacteria Behavior

The protocol used to evaluate MRSA (ATCC 43300) and *P. aeruginosa* (ATCC 27583) behavior on the c.p. Ti substrates, non-coated and coated with SPEEK, is described in Figure 1. Bacteria behavior was studied following the method already described by the authors in [39]. To that aim, a bacterial solution was first prepared from a single individual bacterial colony inoculated into 3% tryptic soy broth (TSB) and cultured into late exponential phase for 24 h at 30 °C with agitation. Then, different solutions were prepared by diluting the solution to a concentration of 10^4 CFU/mL (referred to as 0 dilution) with TSB at 0.3%. The optical density of each solution was measured at 600 nm using a plate reader (SpectraMax M3 equipped with the SoftMax Pro 6.2.2 software, of Molecular Devices, CA, USA). The initial concentration was selected considering three main factors: the values reported in daily life, the minimum number of bacteria sensitive to the porosity, and the counting techniques used.

Bacterial behavior was also studied by immersing the samples into 1.5 mL of a bacteria solution (concentration of 10^4 CFU/mL, referred as −0 dilution) in a 24-well plate and cultured for 3 h at 37 °C. Afterwards, the substrates were rinsed with phosphate buffered saline (PBS) three times. Next, samples were immersed in centrifuge tubes containing 50 mL of PBS, sonicated for 5 min, and vortexed to release the bacteria from the surface and the pores. Then, the PBS solution, having the released bacteria, was diluted to 1:10 (−1 dilution) and 1:100 (−2 dilution). After that, 5 drops of 10 µL of each dilution were deposited on agar plates and dried for 15–20 min. Finally, they were incubated for around 20 h at 37 °C, and bacteria colonies were counted. Three different dilutions of both bacterial strains were tested for each type of c.p. Ti substrate. This process was repeated 3 times for both bacteria strains, MRSA and *P. aeruginosa*, and was performed in duplicate at every step. Furthermore, the MRSA strain at three different concentrations was also analyzed on SPEEK-coated substrates. Finally, a live/dead assay, (LIVE/DEAD® *BacLight*™ Thermofisher, Waltham, MA, USA) for the porous substrates as performed using MRSA and PA with a −0 bacteria dilution. Briefly, samples seeded with MRSA or PA were

washed 5 times with PBS and incubated in dark conditions for 15 min with an equal solution of SYTO and propidium previously prepared in PBS. After that, samples were rinsed 3 times with PBS, and samples were evaluated under confocal microscopy (Leica SP8, Wetzlar, Germany). The quantification of the fluorescence signal was performed on each independent channel following a threshold, and the mean intensity of the green and red fluorescence was measured using Image J software (version 1.51, NIH image, Bethesda, MD, USA).

2.5. Statistical Analysis

In general, each experiment was performed in triplicate using two samples per condition. A one-way ANOVA and a post-Tukey's analysis were performed for bacteria experiments. A P value of <0.01 was deemed to be statistically significant.

3. Results and Discussion

3.1. Titanium Substrate Characterization: Microstructural and Mechanical Properties

Figure 2 shows the SEM, confocal and M-CT images of the porous substrates (100–200, 250–355, and 355–500 μm). The different techniques used in this work provide a complete overview of the porosity distribution at different spatial scales, from an SEM image of the surface samples to a 3D reconstruction by M-CT. For instance, SEM images presented details of the surface roughness inside the pores, while confocal laser and M-CT provided two- and three-dimensional information. This information was essential to determine the inner area and distribution of pores, as well as the roughness within the pores. The main roughness parameters obtained by the confocal laser are summarized in Table 1. The porous c.p. Ti substrates presented different types of pores and sizes. Some micro-pores are inherent to the sintering process (<50 μm), while macro-pores (≥50 μm) are associated with the spacer size used (see red arrow for small pores in confocal images of Figure 2). The values of total porosity were slightly lower than the 50% estimated in the design, since it was the percentage used for the spacer holder and the c.p. Ti powder. Indeed, the lower small porosity level obtained in this study, related to 46 to 47% was already reported in other studies by the authors [36,38] and can be attributed to the small traces of the spacer that were trapped during manufacturing in the isolated porosity.

The low percentage, morphology and size of the micro-pores presented in these samples should not have a representative role on the mechanical properties nor bacterial behavior compared to the macro-pores associated with the spacer particles.

Confocal and SEM images revealed the presence of a micro-scale roughness pattern within the pores (Figure 2). The surface roughness inside the pores increased from 15 to 30 μm with the size of the spacer particles, which were in size ranges of 100–200, 250–355 and 355–500 μm. Regarding the roughness values found for the flat surface, the porous substrates with a higher pore size (355–500 μm) or fully-dense showed an exceptionally smooth surface, revealing an arithmetic mean value of surface roughness, S_a, of 0.7 μm due to the polishing treatment [40]. However, the porous substrates of lower pore sizes (100–200 and 250–355 μm) showed S_a values of 5.0 and 3.4 μm, respectively, which were slightly rougher compared to the polished fully dense sample. The irregular morphology and surface roughness of the spacer particles as well as their fracture during the compaction process may have affected the roughness of the surface inside the pores (the spacer shape was replicated in the titanium matrix, leaving an inner roughness, as observed in SEM images; Figure 2) compared to the pores obtained by conventional PM [43,44]. Many studies have evaluated the role of surface roughness as a key factor for the adhesion and proliferation of bacteria and mammalian cells [45–47]. Indeed, previous studies have confirmed the role of porosity and surface roughness inside pores on cell differentiation and osteoblast adhesion [14,16,39,40]. The roughness values observed inside the pores have been shown to stimulate osteoblast adhesion but also bacteria proliferation and biofilm formation [39,40]. Though roughness is desirable for the improvement of osseointegration, it is not recommended if the intention is to avoid the adhesion and colonization of bacteria on porous structures.

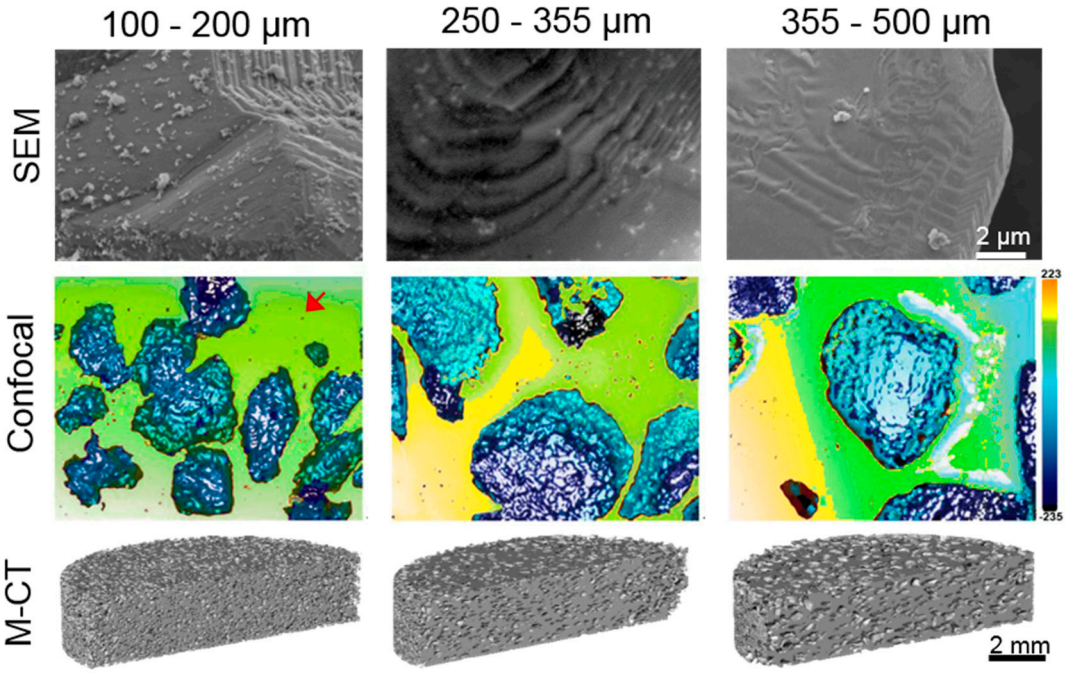

Figure 2. SEM, confocal microscopy and micro-computed tomography (M-CT) images of porous substrates for the different ranges of spacer particle size (100–200, 250–355 and 355–500 µm) showing the surface and pore morphology. Common scale-bar for each type of image.

Table 1. Total porosity measured by image analysis (IA) and roughness parameters determined using confocal laser microscopy of fully-dense and porous substrates.

Samples	*PT* (%)	Confocal Laser					
		Flat Surface			Pore Surface		
		S_a (µm)	S_q (µm)	S_z (µm)	S_a (µm)	S_q (µm)	S_z (µm)
Fully-Dense	2.9	0.6	10.5	78.4		-	
(100–200) µm	47.0	5.0	9.0	97.6	15.5	22.2	166.7
(250–355) µm	46.4	3.4	8.8	147.2	30.8	4.0	274.2
(355–500) µm	46.1	0.7	11.0	79.2	26.7	36.0	485.2

Regarding the M-CT results, which are compiled in Figure 3, different information was obtained, such as the roughness volume percentage of the eroded pore compared to the virtually smoothed pore in dependence of the pore equivalent diameter. These data were extracted from the topographical analysis according to Yin et al. [48] and allowed for the quantification of the surface roughness inside the pores. In addition, the total inner surface was calculated from analyzing an M-CT representative fraction of the total sample volume (Table 2). It is worth mentioning that the larger the spacer particles, the rougher the surface inside the pores (i.e., for a pore size of 355–500 µm, the roughness value by volume was 37 mm^3, higher than the 18 mm^3 estimated for the 100–200 µm pore size). However, the probability that the bacteria will find these rough areas decreased (as measured in terms of percentage of roughness), as can be seen in Figure 3 and in the confocal images of Figure 2. For the same porosity percentage, the substrate with larger pores presented less pores per area; therefore, the mean free path between pores was larger. In fact, the influence of topography and the impact on bacteria adhesion has already been reported [49]. In this context, Bevilacqua and co-workers evaluated the effect of roughness of different titanium surfaces on *P. aeruginosa* and MSB (mix salivary bacteria), and they observed a clear effect of roughness on early adhesion states (24 h of bacteria incubation) but not after biofilm formation at four days [11]. Whitehead and co-workers saw that the architecture of

surface in terms of roughness values, geometry of topography, and the size of these micro or nanoscale features may determine the retention of bacteria [50].

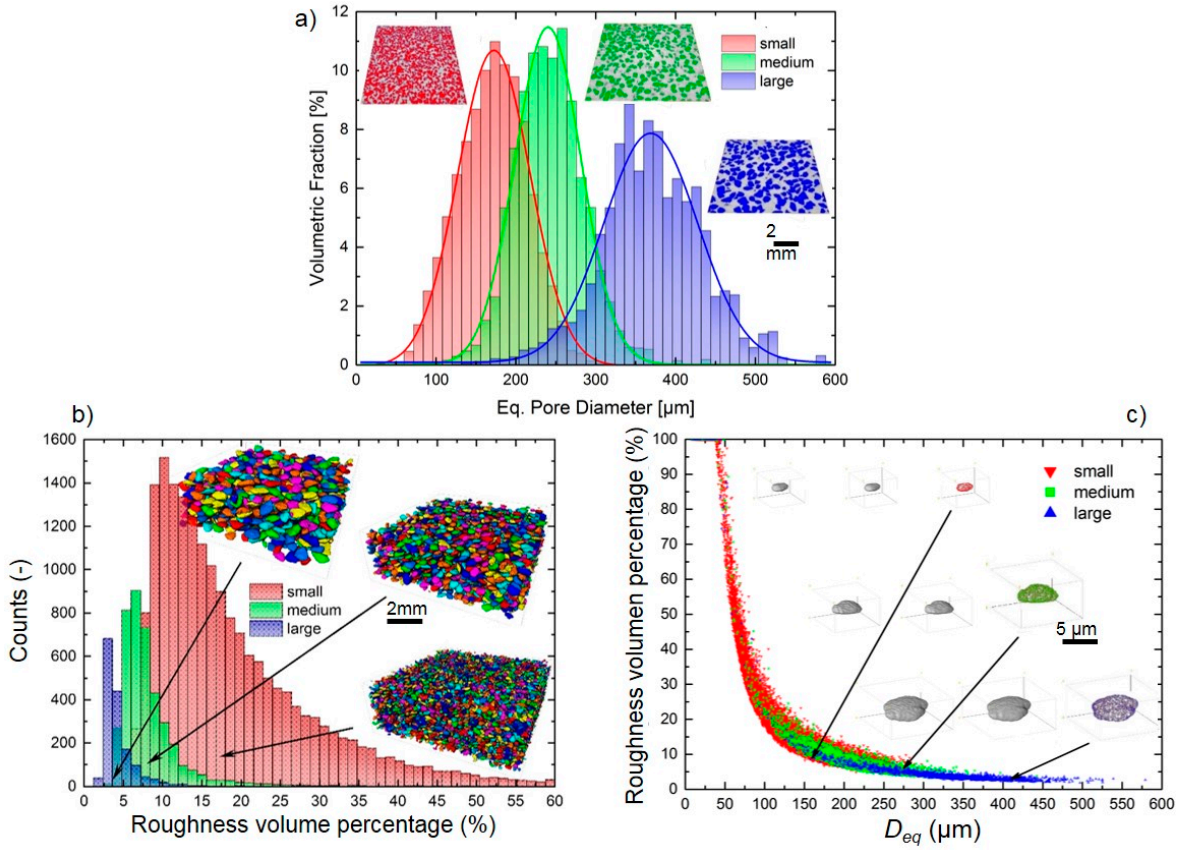

Figure 3. Distributions of different M-CT parameters for the three studied porous substrates (100–200, 250–355, and 355–500 µm): (**a**) D_{eq} vs. volume fraction, (**b**) distribution of the roughness volume percentage, and (**c**) D_{eq} vs. roughness volume percentage. Inset: A rippled pore, the smoothed one and the volume difference marked in color.

Table 2. Microstructural characterization of porous substrates using M-CT analyses.

Spacer Size (µm)	Surface/Volume (mm^2/mm^3)	Estimated		
		Flat Area (mm^2)	Porous Area (mm^2)	Volume (mm^3)
100–200	17.3 ± 1.3	54.0 ± 13.8	321.0 ± 44.8	18.6 ± 1.2
250–355	10.7 ± 0.8	59.9 ± 17.5	260.1 ± 29.6	24.3 ± 0.9
355–500	8.4 ± 0.6	50.8 ± 11.9	311.9 ± 29.9	37.1 ± 0.8

Figure 4 shows the stress–strain curve for the porous substrates. E_c and σ_y were determined for all of them, revealing an inverse relationship between the total porosity and size of the pores. The stiffness values obtained for the porous c.p. Ti samples were adapted to the requirements of natural bone tissue (20–25 GPa), whereas the mechanical strength values were lower (150–180 MPa). This reduction of mechanical strength was more representative, as expected, for larger pores. However, this problem could be compensated by the growth of bone tissue towards the inner part of the implant and the improvement of adhesion of osteoblast cells, a phenomenon that could be favored by the increase in the size and degree of interconnectivity of the pores.

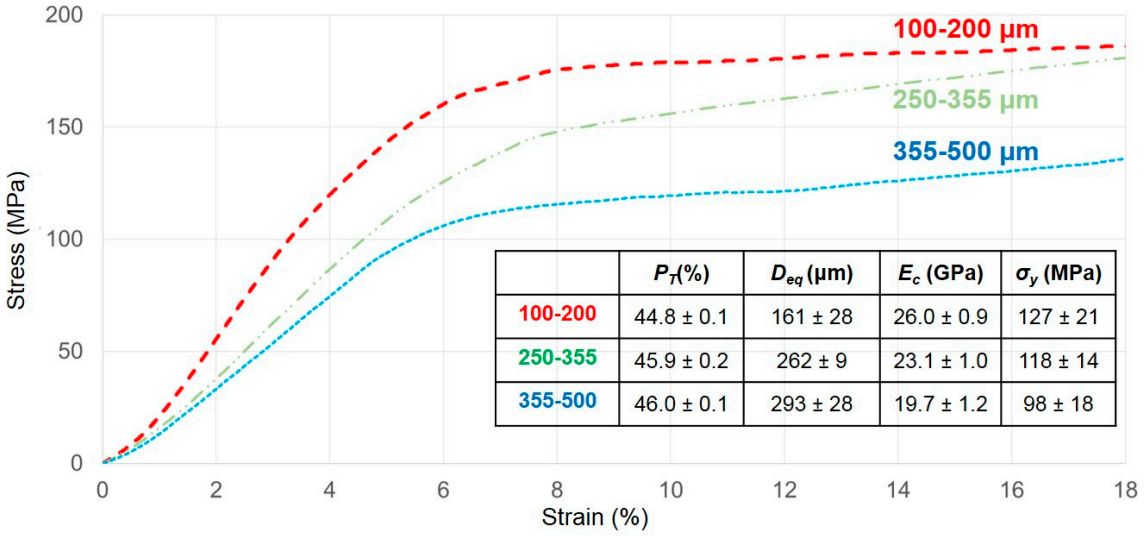

	P_T(%)	D_{eq} (µm)	E_c (GPa)	σ_y (MPa)
100-200	44.8 ± 0.1	161 ± 28	26.0 ± 0.9	127 ± 21
250-355	45.9 ± 0.2	262 ± 9	23.1 ± 1.0	118 ± 14
355-500	46.0 ± 0.1	293 ± 28	19.7 ± 1.2	98 ± 18

Figure 4. Stress–strain curve of the three porous titanium substrates. Inset: Parameters obtained from Archimedes' method (P_T and D_{eq}) and uniaxial compression test (Young's modulus (E_c) and yield strength (σ_y)).

Furthermore, Figure 5a,b shows the representative micro-mechanical loading–unloading curves (using static and dynamic conditions) of the titanium substrates. In addition, the results plotted in Figure 5c,d display the calculated micro hardness and stiffness for the tested samples as a function of penetration depth. On the other hand, Figure 6 shows the hardness and stiffness values obtained by different methods, i.e., stiffness calculated from uniaxial compression tests and ultrasonic techniques. Additionally, the Young's modulus was also estimated using Equation (4), as proposed by Nielsen [51]:

$$E_N = \frac{E_o \cdot (1-P)^2}{1 + \left(\frac{1}{f} - 1\right)P} \tag{4}$$

From these data, some statements can be confirmed:

1. For the same maximum load, the penetration depth and elastic recovery was higher for porous samples (see Table 3), particularly for the substrate with a lower mean free path between the pores (higher effect of the porosity). The direct relationship between porosity and elastic recovery is widely accepted in the literature [38,52].
2. Regardless of the type of substrate, the micromechanical properties depended on the value of the applied load and the mode of application of these local phenomena of micro plasticity and hardening. The influence of the tip of the indenter, the surface roughness, the sensitivity of the load cell and the linear variable differential transformer, etc., must also be considered.
3. Independent of the maximum applied load, micro-hardness and stiffness increased with the mean free path and, thus, with the size of the Ti matrix where indentation was performed. This fact means that the influence of porosity was less pronounced in micro-mechanical properties compared to the fully-dense c.p. Ti substrates (which had a porosity of 2.9 vol. %).
4. It should be noticed that, although the values of hardness and stiffness differed, that a similar tendency was observed: Both properties increased with the mean free path in porous Ti substrates, but they were always lower than in the case of the fully-dense c.p. Ti substrate.
5. The differences observed for the stiffness values could be associated with the volume of material involved in each type of test (the influence of the porosity and plasticity phenomena), deformation speed, and/or test limitations (rigidity of testing machine, precision, etc.).

6. The inverse tendencies of the micro-hardness values and *E* with the applied load in the dynamic tests was generally expected, as were the values obtained in the plateau zone (corroborant the role of porosity), as was discussed above.

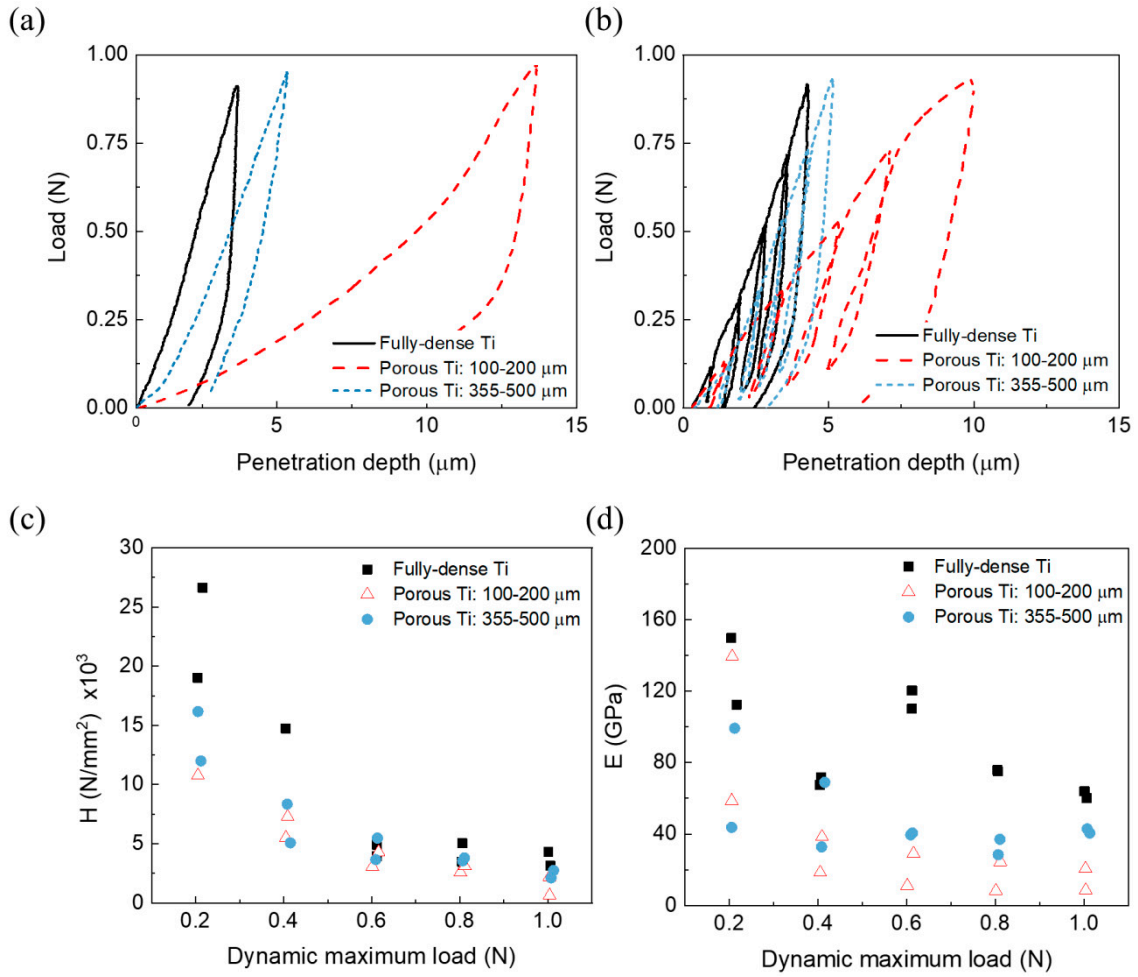

Figure 5. Instrumented micro-indentation of fully-dense and porous titanium substrates: (**a**) Loading–unloading curves (*P-h* curves) under static and (**b**) dynamic loads, as well as the (**c**,**d**) mechanical properties (micro-hardness and Young's modulus) as a function of penetration depth (dynamic conditions).

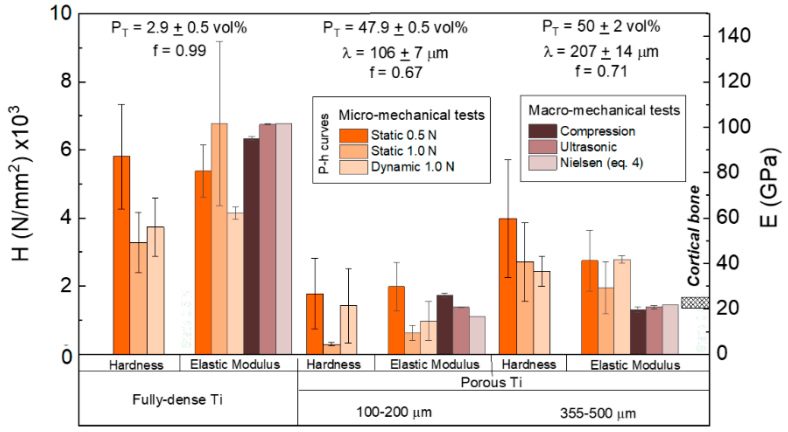

Figure 6. Macro- and micro-mechanical behavior as obtained by different techniques.

Table 3. Characteristic parameters of loading–unloading curves and pseudo-creep behavior evaluated by micro-indentation tests.

Samples	Static Micro-Indentation Tests			Pseudo-Creep Behavior	
	h_{max} (μm)	Elastic Recovery		Plateau, Δh (μm)	Penetration Depth Rate (μm/s) $\times 10^{-4}$
		Absolute (μm)	Relative (%)		
Fully-dense	4.3 ± 0.7	1.9	44	0.7	2.5
(100–200) μm	15 ± 4	7.1	47	0.8	1.4
(355–500) μm	7 ± 3	3.4	48	0.5	0.83

Finally, results associated with the pseudo-creep behavior of the substrates are presented in Figure 7 and Table 3, which evaluate the role of porosity. Figure 7 shows both the plateau size (absolute strain during the holding time) and the penetration depth rate, which were higher for the substrates obtained with a size range of spacer particles between 100 and 200 μm. This effect was related to the mean free path of the samples; i.e., porous titanium substrates with a higher mean free path (higher residual Ti matrix between the pores) behaved closer to the fully-dense c.p. Ti.

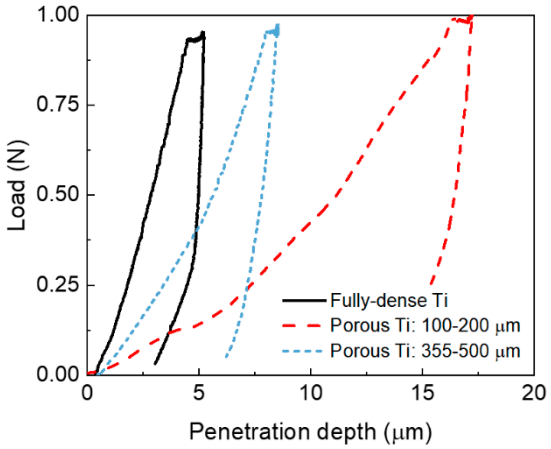

Figure 7. Pseudo-creep behavior of fully-dense (in black) and porous Ti (in red and blue, respectively) substrates.

3.2. *Evaluation of Bacterial Behavior on Fully and Porous Substrates with and without SPEEK Coating*

The results obtained from the analyses of MRSA and *P. aeruginosa* behavior onto raw c.p. Ti non-coated surfaces (see protocol in Figure 1), both absolute and normalized by the total surface area values, are presented in Figure 8 for the −1 dilution. Indeed, the bacteria proliferation for the 0 dilution were non-quantifiable. Studies of MRSA and *P. aeruginosa* behavior revealed that the presence of pores promotes bacterial proliferation and sees an increase in CFU compared to fully-dense c.p. Ti was observed. The former illustrated a higher number on CFU in porous substrates per area than in fully-dense substrates, which correlated to high bacteria density on the porous samples. The growth of MRSA and *P. aeruginosa* was influenced by pore size. For both strains, the proliferation was greater in higher ranges of spacer particles sizes, reaching similar values for both the 250–355 and 355–500 μm ranges. Whitehead and co-workers suggested that the presence of grooves, spacers between grooves, and the size of the groove may promote bacteria adhesion on titanium surfaces [50]. In that sense, the three porous structures, 100–200, 250–355, and 355–500 μm, presented wrinkles inside the pores (see the SEM images in Figure 2) and a smooth flat surface between pores. This complex surface offered an attractive roughness inside the pores due to the presence of the wrinkles and, in the case of larger pore substrates (355–500 μm), a higher number of attached bacteria was quantified. In addition, the larger open pore diameters in the 355–500 μm sample allowed the bacteria to reach the pore surface

and be kept in the pores more easily. However, the smoother surface for the fully dense samples did not promote the adhesion of bacteria, and a reduced CFU was observed.

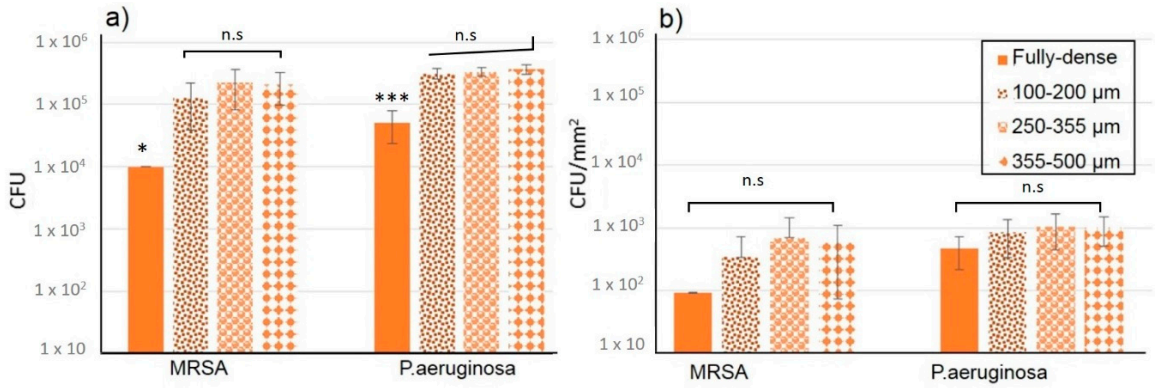

Figure 8. Bacterial behavior for different MRSA and *P. aeruginosa* bacteria concentrations on titanium substrates: (**a**) Absolute values and (**b**) normalized values per area. Note: Data are expressed as the mean ± standard error of the mean. * $P < 0.05$, ** $P < 0.01$ (compared to all others).

Apart from the bacteria concentration and porosity evaluation on MRSA and PA behavior by counting colony-forming units, a live and dead study was performed in order to evaluate the presence of live bacteria on flat surfaces and inside pores of the different porous substrates. Since it has been reported that surface chemistry is not the only material property that plays a key role in bacteria adhesion because roughness and topography also affect bacteria attachment and subsequently biofilm formation, the samples were also analyzed by confocal microscopy (Figure 9).

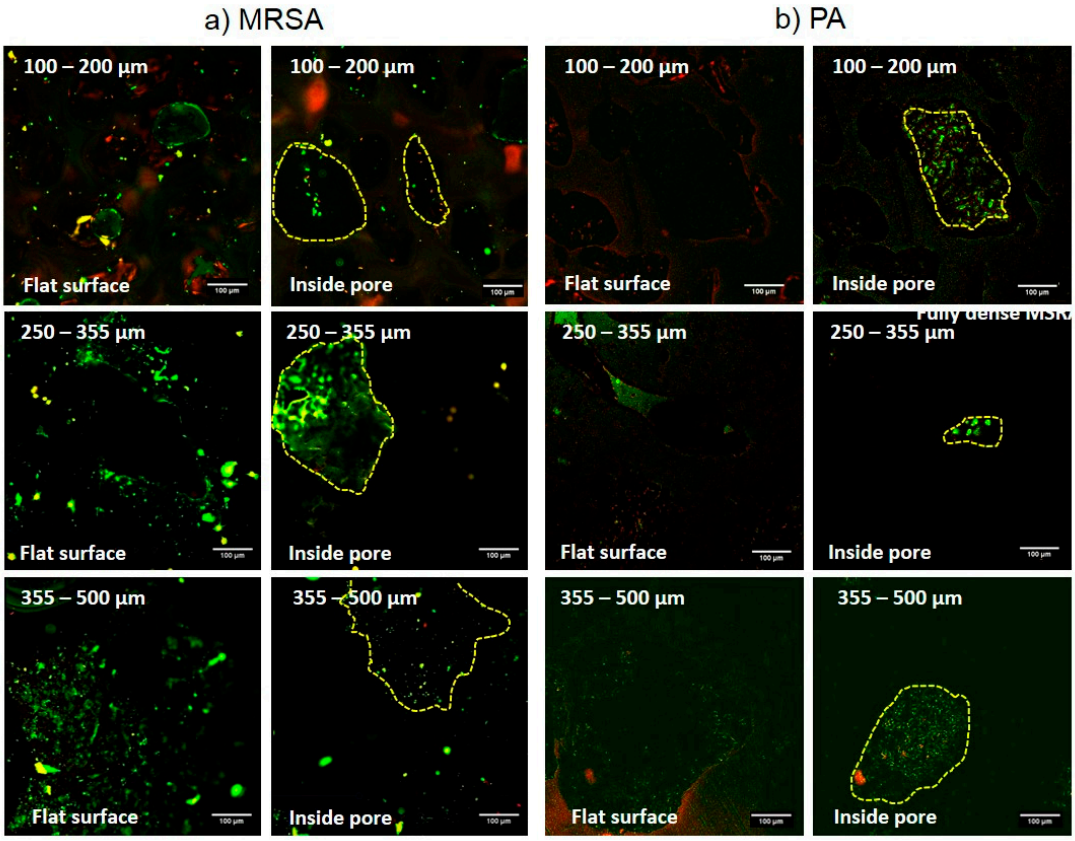

Figure 9. Confocal microscopy study of live and dead MRSA (**a**) and PA (**b**) on flat and pore surfaces for the three different porous uncoated substrates. Green fluorescence represents alive bacteria, while red dots represents dead bacteria and yellow damaged cells.

In these confocal images, the flat surfaces for all of the porous substrates showed higher numbers of alive cells for both bacteria strains. However, the damaged or dead cells on flat surfaces were higher than in the surface inside the pores, highlighting the small spacer particle size of 100–200 µm as the porous substrates with the best performance to reduce alive MRSA and PA bacteria on flat and pore surfaces. Furthermore, this bacteria behavior observed using 100–200 µm porous scaffolds was similar with *P. aeruginosa* and thus confirmed the fluorescence values measured by the Image J software (see Figure 10). This particular spacer particle size offered the highest dead cell fluorescence and the lowest fluorescence level of alive bacteria for both cell lines on a flat surface. Inside the pores, for example, for the 250–355 µm substrate, a high green fluorescence intensity could be observed, so the amount of dead bacteria was very low. For the highest particle spacer size (355–500 µm), the exposed surface and the presence of larger pores offered a rougher surface in which alive bacteria (MRSA and PA) could attach and grow better than the surface offered for the 100–200 µm samples. Therefore, the topography of uncoated, pristine surfaces revealed different bacteria behavior on flat smooth surfaces than inside the pores; it also revealed the larger particle size as the aspect of porous substrates that could easily favor increased bacteria survival and biofilm formation.

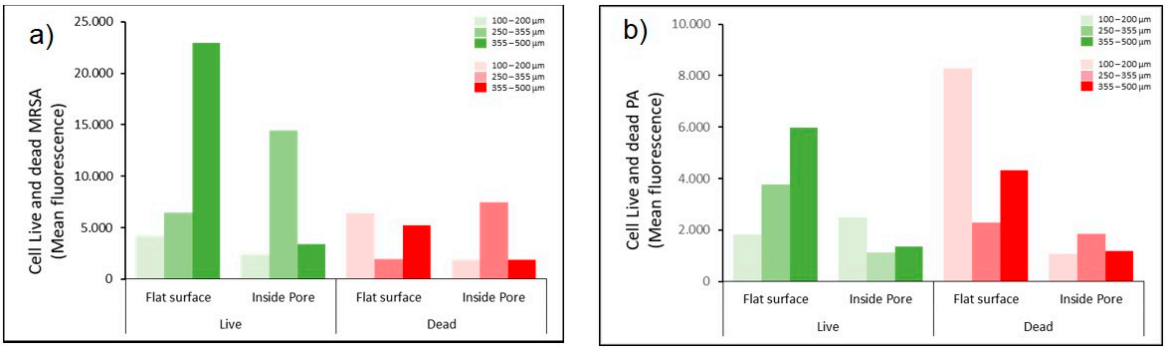

Figure 10. Quantification of fluorescence intensity of confocal images for the three different substrates for both cell lines MRSA (**a**) and PA (**b**). Results are expressed as the mean of the fluorescence intensity signal measured using Image J software.

To confirm the antibiofouling activity of the SPEEK coating and to include a chemical surface modification as an interesting strategy to reduce or control bacterial infection on porous substrates, SPEEK-coated and uncoated porous surfaces were compared. In this experiment, a surface modification based on the application of SPEEK onto porous titanium substrates was performed, and the synthesis and characterization of the SPEEK coating was evaluated (Figure 11). From a macroscopic point of view (Figure 11a,b), a thin SPEEK coating was observed, and the coating did not fully cover the pores of the porous substrates. The presence of this coating was confirmed in the SEM images, using c.p. Ti substrates as clear examples. A scratch was performed on c.p. fully Ti-SPEEK to show a thin and homogeneous SPEEK film (Figure 11d). In addition, EDS results showed the presence of sulphur groups on the coated substrate (see Figure 11f) compared to the lack of this signal in the Ti non-coated samples. All these results confirmed the successful development of the SPEEK coating onto fully-dense and porous c.p. Ti substrates. This polymeric coating has been previously evaluated in terms of cell biocompatibility and osteoblast differentiation in several studies [53,54]. As a bioactive coating, putting SPEEK onto titanium substrates has shown suitable properties for bone and dental applications as well as for reducing bacterial infections [53].

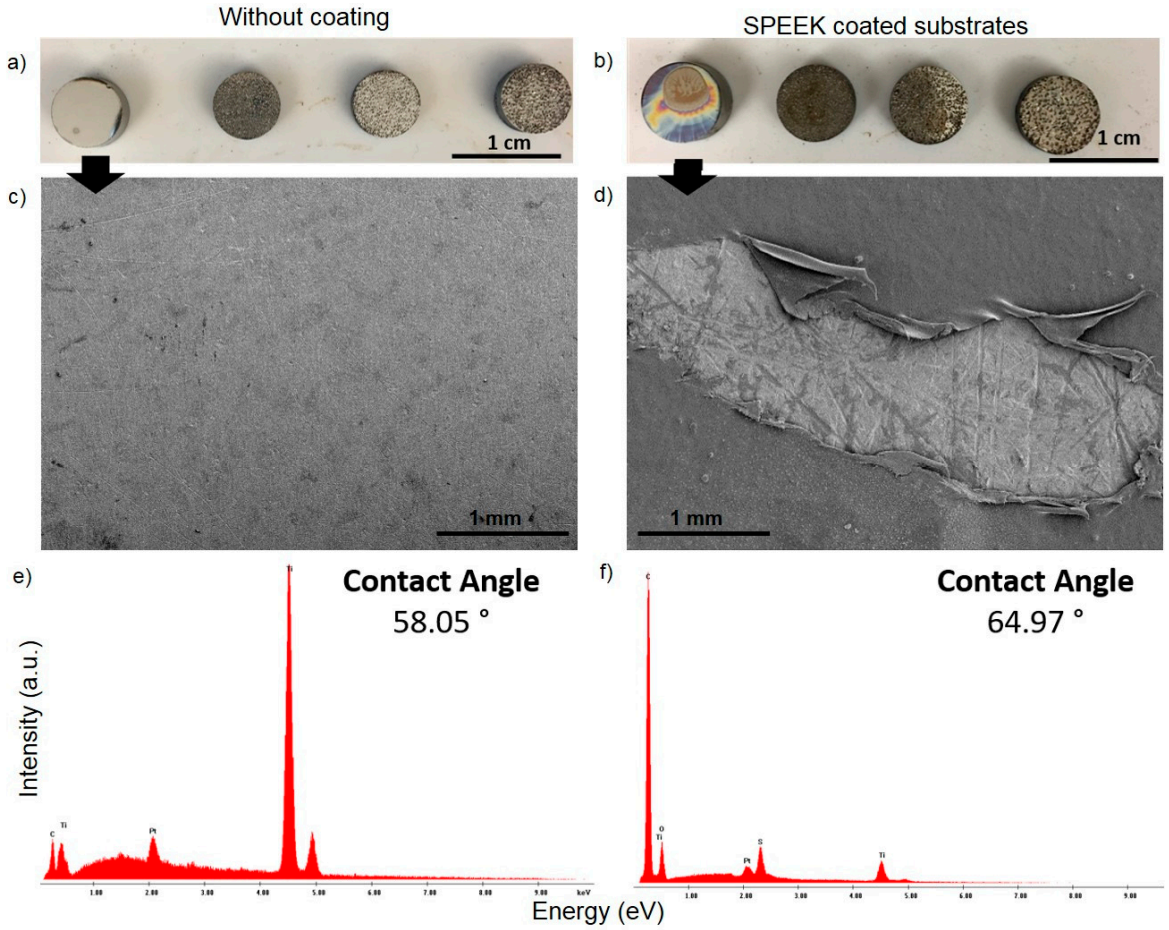

Figure 11. Topography and chemistry surface evaluation of SPEEK coating. Macro-photography of the coated and non-coated samples revealed the presence of the coating (**a**,**b**), which was confirmed by SEM images of the fully dense surface (**c**,**d**). A scratch performed in the SPEEK fully-dense samples showed a thin and homogeneous SPEEK film. An energy dispersive spectroscopy (EDS) analysis corroborated the presence of sulfur groups in SPEEK-coated samples as well slightly increased contact angle values due to the increase in sulfur groups in the PEEK structure (**e**,**f**).

Regarding bacteria adhesion and colonization behavior, macro-photography of the colony forming-units using MRSA for coated and non-coated fully-dense and porous c.p. Ti substrates was conducted (Figure 12). For the non-coated samples, the presence of pores compared to flat smooth surfaces showed different bacteria behavior. A reduction of CFU for the same substrates was also observed in fully dense Ti and the 100–200 µm porous substrates. The presence of pores of a higher size promoted biofilm formation, as observed in the agar plates of higher colony formation. In contrast, it was remarkable to see the effect of SPEEK coating in reducing the number of colony formation for all samples—not only for the fully dense but also for the porous substrates, thus confirming the antibiofouling property of this coating. As seen in Figure 12, the SPEEK coating on MRSA behavior revealed decreased bacteria proliferation on all the samples, especially on the porous substrates. The SPEEK coating showed that bacterial growth was significantly inhibited on all porous samples and for all bacteria concentrations. These findings are related due to a combination of diverse factors. On the one hand, the SPEEK coating fills in the cavities, reducing the roughness inside the pores and closing some of them, therefore avoiding the entry of bacteria. On the other hand, this coating has antibiofouling properties due to the composition of the SPEEK coating, which is based on S-content. Montero and co-workers evaluated the degree of sulfonation on bacteria biofilm formation, and they observed that more than two-to-three hours of sulfonation reduced biofilm formation [53], which can also be seen in Figure 12 due to the absence of colonies in the agar plates. Though the role of sulfur

on the bioactivity could be questioned, several reports have confirmed that sulfonation treatment followed by simulated body fluid incubation had a significant positive impact on osteointegration [55]. Related to mechanical properties, the fact that the coating fills in the pores should not be representative on the stiffness of the substrates, even it could be positive in terms of fatigue resistance.

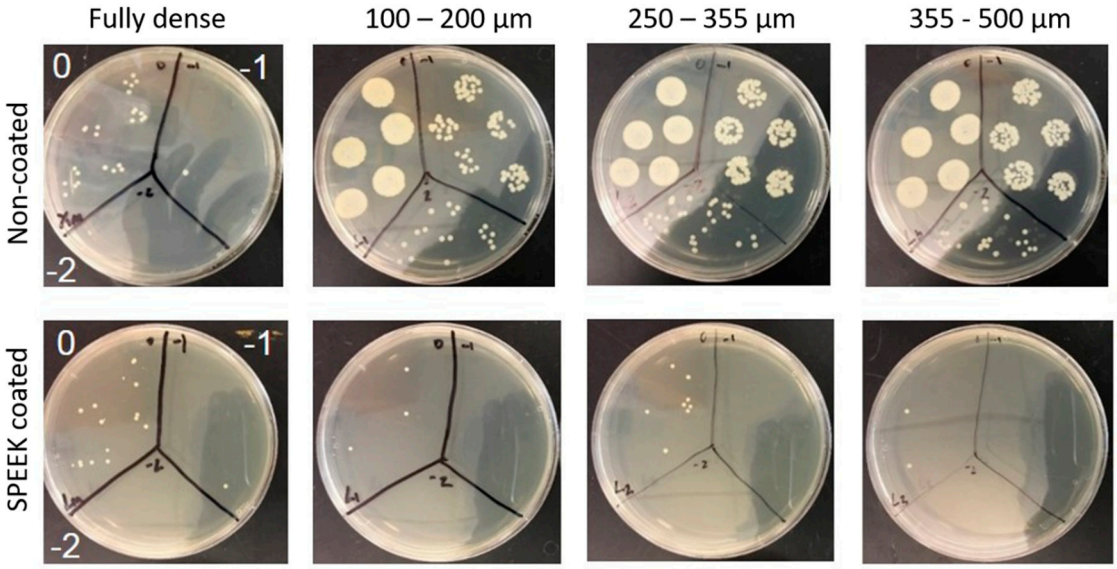

Figure 12. Colony-forming units for MRSA for the different coated and uncoated substrates (fully-dense and porous Ti-substrates with different ranges of spacer particle sizes). Macro-photography of CFU numbers grown in agar plates using three different concentrations (0, −1 and −2 dilutions) reproduced from [39], with permission from Elsevier, 2019.

4. Conclusions

This work evaluated the role of porosity to achieve a better biomechanical and antibacterial equilibrium for coated fully-dense and porous c.p. Ti substrates for partial bone replacements. Concerning macro- and micro-mechanical behavior, an inverse relationship between the mean free path (Ti matrix size) and the Young´s modulus, micro-hardness and the pseudo-creep effects (strain rate at constant load) was observed. In fact, porous c.p. Ti substrates had a higher mean free behavior closer to the fully-dense c.p. Ti. Furthermore, the studies of the bacteria behavior revealed that the pores promoted bacterial attachment and proliferation, highlighting an increase in larger pore sizes (250−355 and 355−500 µm). The use of a SPEEK coating treatment presented important anti-bacterial abilities; this coating inhibited MRSA adhesion and growth, especially in the porous substrates, mainly for larger sizes of pores. The SPEEK coating had a similar bactericide effect for all substrates. In summary, among the different substrates studied, the one with smaller pore sizes (100−200 µm) can be considered the most suitable one, since this range of pores sizes can assure the best bio-mechanical (stiffness, HV, yield strength and creep resistance) and biofunctional (allowing for bone in-growth and the infiltration of the SPEEK coating, as well as suggesting a potential improvement of osseointegration) balance.

Author Contributions: Conceptualization, project administration and supervision: T.J.W., J.A.R.-O. and Y.T.; investigation, formal analysis and validation: A.M.B., A.C., C.D.-T., R.M., A.M.R., F.G.-M. and P.H.K. discussion and writing—original draft preparation, all the authors.

Funding: This research was funded by Ministry of Economy and Competitiveness of Spain under the grant MAT2015-71284-P.

Acknowledgments: The authors dedicate this paper to the memory of Juan J. Pavón Palacio (University of Antioquia, Colombia). AMB also thanks the financial support of the University of Seville for the research stay at Institute of Applied Materials, Helmholtz-Zentrum Berlin für Materialien und Energie, Berlin (Germany) (Grant: VI Plan Propio de Investigación y Transferencia—US 2018, I.3A2).

Conflicts of Interest: The authors declare no conflict of interest.

References

1. Kurtz, S.M.; Ong, K.L.; Lau, E.; Bozic, K.J.; Berry, D.; Parvizi, J. Prosthetic joint infection risk after TKA in the Medicare population. *Clin. Orthop. Relat. Res.* **2010**, *468*, 52–56. [CrossRef] [PubMed]
2. Lafaurie, G.I.; Sabogal, M.A.; Castillo, D.M.; Rincón, M.V.; Gómez, L.A.; Lesmes, Y.A.; Chambrone, L. Microbiome and microbial biofilm profiles of peri-implantitis: A systematic review. *J. Periodontol.* **2017**, *88*, 1066–1089. [CrossRef] [PubMed]
3. Derks, J.; Tomasi, C. Peri-implant health and disease. A systematic review of current epidemiology. *J. Clin. Periodontol.* **2015**, *42*, S158–S171. [CrossRef] [PubMed]
4. Liu, R.; Tang, Y.; Zeng, L.; Zhao, Y.; Ma, Z.; Sun, Z.; Ren, L.; Yang, K. In vitro and in vivo studies of anti-bacterial copper-bearing titanium alloy for dental application. *Dent. Mater.* **2018**, *34*, 1112–1126. [CrossRef] [PubMed]
5. Zhao, L.; Wang, H.; Cu, L.; Zhang, W.; Ni, H.; Zhang, Y.; Wu, Z.; Chu, P.K. Antibacterial nano-structured titania coating incorporated with silver nanoparticles. *Biomaterials* **2011**, *32*, 5706–5716. [CrossRef] [PubMed]
6. Cheng, L.; Weir, M.D.; Xu, H.H.; Antonucci, J.M.; Kraigsley, A.M.; Lin, N.J.; Lin-Gibson, S.; Zhou, X. Antibacterial amorphous calcium phosphate nanocomposites with a quaternary ammonium dimethacrylate and silver nanoparticles. *Dent. Mater.* **2012**, *28*, 561–572. [CrossRef] [PubMed]
7. Dhir, S. Biofilm and dental implant: The microbial link. *J. Indian Soc. Periodontol.* **2013**, *17*, 5–11. [CrossRef] [PubMed]
8. Soloaga, R.; Corso, A.; Gagetti, P.; Faccone, D.; Galas, M. Detección de meticilino-resistencia en Staphylococcus aureus: Comparación de métodos convencionales y aglutinación con mrsa-Screen latex. *Rev. Argent. Microbiol.* **2004**, *36*, 36–40. [PubMed]
9. Gleva, M.; Arxé, D. Do you know the MARSA? Do you know how to act against MARSA? (original title: ¿Conoces el MARSA? ¿Sabes cómo actuar delante de un MARSA?). *El Peu* **2005**, *25*, 126–131.
10. Montero, M. Pseudomonas Aeruginosa Multiresistente: Aspectos Epidemiológicos, Clínicos y Terapéuticos. Ph.D. Thesis, Universidad Autonoma de Barcelona, Barcelona, Spain, 2012.
11. Bevilacqua, L.; Milan, A.; Del Lupo, V.; Maglione, M.; Dolzani, L. Biofilms developed on dental implant titanium surfaces with different roughness: Comparison between in vitro and in vivo studies. *Curr. Microbiol.* **2018**, *75*, 766–772. [CrossRef]
12. Kunčická, N.; Kocich, R.; Lowe, T.C. Advances in metals and alloys for joint replacement. *Prog. Mater. Sci.* **2017**, *88*, 232–280. [CrossRef]
13. Niinomi, M. Mechanical biocompatibilities of titanium alloys for biomedical applications. *J. Mech. Behav. Biomed. Mater.* **2008**, *1*, 30–42. [CrossRef] [PubMed]
14. Torres, Y.; Pavón, J.J.; Rodríguez-Ortiz, J.A. Processing and characterization of porous titanium for implants by using NaCl as space holder. *J. Mater. Process. Technol.* **2012**, *212*, 1061–1069. [CrossRef]
15. Torres, Y.; Pavón, J.J.; Nieto, I.; Rodríguez-Ortiz, J.A. Conventional powder metallurgy process and characterization of porous titanium for biomedical applications. *Metall. Mater. Trans. B Process. Metall. Mater. Process. Sci.* **2011**, *42*, 891–900. [CrossRef]
16. Muñoz, S.; Pavón, J.J.; Rodríguez-Ortiz, J.A.; Civantos, A.; Allain, J.P.; Torres, Y. On the influence of space holder in the development of porous titanium implants: Mechanical, computational and biological evaluation. *Mater. Charact.* **2015**, *108*, 68–78. [CrossRef]
17. Jurczyk, M.U.; Jurczyk, K.; Miklaszewski, A.; Jurczyk, M. Nanostructured titanium-45S5 Bioglass scaffold composites for medical applications. *Mater. Des.* **2011**, *32*, 4882–4889. [CrossRef]
18. Torres, Y.; Rodrıguez-Ortiz, J.A.; Arias, S.; Echeverry, M.; Robledo, S.; Amigo, V.; Pavón, J.J. Processing, characterization and biological testing of porous titanium obtained by space-holder technique. *J. Mater. Sci.* **2012**, *47*, 6565–6576. [CrossRef]
19. Pałka, K.; Pokrowiecki, R. Porous Titanium Implants: A Review. *Adv. Eng. Mater.* **2018**, *2018*, 1–18. [CrossRef]
20. Tande, A.J.; Patel, R. Prosthetic joint infection. *Clin. Microbiol. Rev.* **2014**, *27*, 302–345. [CrossRef]
21. Smith, A.W. Biofilms and antibiotic therapy: Is there a role for combating bacterial resistance by the use of novel drug delivery systems? *Adv. Drug Deliv. Rev.* **2005**, *57*, 1539–1550. [CrossRef]

22. Taheri, S.; Cavallaro, A.; Christo, S.N.; Smith, L.E.; Majewski, P.; Barton, M.; Hayball, J.D.; Vasiev, K. Substrate independent silver nanoparticle based antibacterial coatings. *Biomaterials* **2014**, *35*, 4601–4609. [CrossRef] [PubMed]
23. Amin-Yavari, S.; Loozen, L.; Paganelli, F.L.; Bakhshandeh, S.; Lietaert, K.; Groot, J.A.; Fluit, A.C.; Boel, C.H.E.; Alblas, J.; Vogely, H.C.; et al. Antibacterial behavior of additively manufactured porous Titanium with nanotubular surfaces releasing Silver ions. *ACS Appl. Mater. Interfaces* **2016**, *8*, 17080–17089. [CrossRef] [PubMed]
24. Jia, Z.; Li, M.; Xiu, P.; Xu, X.; Cheng, Y.; Zheng, Y.; Xi, T.; Wei, S.; Liu, Z. A novel cytocompatible, hierarchical porous Ti6Al4V scaffold with immobilized silver nanoparticles. *Mater. Lett.* **2015**, *157*, 143–146. [CrossRef]
25. Rtimi, S.; Baghriche, O.; Pulgarin, C.; Ehiasarian, A.; Bandorf, R.; Kiwi, J. Comparison of HIPIMS sputtered Ag- and Cu-surfaces leading to accelerated bacterial inactivation in the dark. *Surf. Coat. Technol.* **2014**, *250*, 14–20. [CrossRef]
26. Rtimi, S.; Sanjines, R.; Andrzejczuk, M.; Pulgarin, C.; Kulik, A.; Kiwi, J. Innovative transparent non-scattering TiO_2 bactericide thin films inducing increased *E. coli* cell wall fluidity. *Surf. Coat. Technol.* **2014**, *254*, 333–343. [CrossRef]
27. Rtimi, S.; Kiwi, J. Bactericide effects of transparent polyethylene photocatalytic films coated by oxides under visible light. *Appl. Catal. B Environ.* **2017**, *213*, 62–73. [CrossRef]
28. Hasan, J.; Crawford, R.J.; Ivanova, E.P. Antibacterial surfaces: The quest for a new generation of biomaterials. *Trends Biotechnol.* **2013**, *31*, 295–304. [CrossRef]
29. Bassegoda, A.; Ivanova, K.; Ramon, E.; Tzanov, T. Strategies to prevent the occurrence of resistance against antibiotics by using advanced materials. *Appl. Microbiol. Biotechnol.* **2018**, *102*, 2075–2089. [CrossRef]
30. Moritz, M.; Geszke-Moritz, M. The newest achievements in synthesis, immobilization and practical applications of antibacterial nanoparticles. *Chem. Eng. J.* **2013**, *228*, 596–613. [CrossRef]
31. Qiao, Y.; Liu, X. Biocompatible Coating. In *Book Comprehensive Materials Processing*; Hashmi, S., Ferreira, G., Van Tyne, C.J., Yilbas, B., Eds.; Elsevier: Amsterdam, The Netherlands, 2014; pp. 425–447. [CrossRef]
32. McGilvray, K.C.; Waldorff, E.I.; Easley, J.; Seim, H.B.; Zhang, N.; Linovitz, R.J.; Ryaby, J.T.; Puttlitz, C.M. Evaluation of a polyetheretherketone (PEEK) titanium composite interbody spacer in an ovine lumbar interbody fusion model: Biomechanical, microcomputed tomographic, and histologic analyses. *Spine, J.* **2017**, *17*, 1907–1916. [CrossRef]
33. Ouyang, L.; Zhao, Y.; Jin, G.; Lu, T.; Li, J.; Qiao, Y.; Ning, C.; Zhang, X.; Chu, P.K.; Liu, X. Influence of sulfur content on bone formation and antibacterial ability of sulfonated PEEK. *Biomaterials* **2016**, *83*, 115–126. [CrossRef] [PubMed]
34. Najeeb, S.; Zafar, M.S.; Khurshid, Z.; Siddiqui, F. Applications of polyetheretherketone (PEEK) in oral implantology and prosthodontics. *J. Prosthodon. Res.* **2016**, *60*, 12–19. [CrossRef] [PubMed]
35. Shuai, C.; Shuai, C.; Feng, P.; Gao, C.; Peng, S.; Yang, Y. Antibacterial capability, physicochemical properties, and biocompatibility of nTiO incorporated polymeric scaffolds. *Polymers* **2018**, *10*, 328. [CrossRef] [PubMed]
36. Dominguez-Trujillo, C.; Peón, E.; Pavón, J.J.; Montealegre-Melendez, I.; Arevalo, C.; Galvan, J.C.; García-Moreno, F.; Torres, Y. Sol-gel deposition of hydroxyapatite coatings on porous titanium for biomedical applications. *Surf. Coat. Technol.* **2018**, *333*, 158–162. [CrossRef]
37. Dominguez-Trujillo, C.; Ternero, F.; Rodriguez-Ortiz, J.A.; Pavón, J.J.; García-Couce, J.; Galvan, J.C.; García-Moreno, F.; Torres, Y. Improvement of the balance between a reduced stress shielding and bone ingrowth by bioactive coatings onto porous titanium substrates. *Surf. Coat. Technol.* **2018**, *338*, 32–37. [CrossRef]
38. Dominguez-Trujillo, C.; Ternero, F.; Rodriguez-Ortiz, J.A.; Heise, S.; Boccaccini, A.R.; Lebrato, J.; Torres, Y. Bioactive coatings on porous titanium for biomedical applications. *Surf. Coat. Technol.* **2018**, *349*, 548–592. [CrossRef]
39. Dominguez-Trujillo, C.; Beltrán, A.M.; Garvi, M.D.; Salazar-Moya, A.; Lebrato, J.; Hickey, D.J.; Rodriguez-Ortiz, J.A.; Kamm, P.H.; Lebrato, C.; García-Moreno, F.; et al. Bacterial behavior on coated porous titanium substrate for biomedical applications. *Surf. Coat. Technol.* **2019**, *357*, 896–902. [CrossRef]
40. Civantos, A.; Domínguez, C.; Pino, R.J.; Setti, G.; Pavon, J.J.; Martínez-Campos, E.; Garcia-Garcia, F.J.; Rodriguez-Ortiz, J.A.; Allain, J.P.; Torres, Y. Designing bioactive porous titanium interfaces to balance mechanical properties and in vitro cells behavior towards increased osseointegration. *Surf. Coat. Technol.* **2019**, *368*, 162–174. [CrossRef]

41. International Standard. *ISO 13314: 2011 (E). Mechanical Testing of Metals—Ductility Testing—Compression Test. for Porous and Cellular Metals, Ref. Number ISO. 13314 (n.d.)*; International Organization for Standardization: Geneva, Switzerland, 2011; pp. 1–7.
42. Oliver, W.C.; Pharr, G.M. Measurement of hardness and elastic modulus by instrumented indentation: Advances in understanding and refinements to methodology. *J. Mater. Res.* **2004**, *19*, 3–20. [CrossRef]
43. Torres, Y.; Trueba, P.; Pavón, J.J.; Chicardi, E.; Kamm, P.; García-Moreno, F.; Rodríguez-Ortiz, J.A. Design, processing and characterization of titanium with radial graded porosity for bone implants. *Mater. Des.* **2016**, *110*, 179–187. [CrossRef]
44. Lascano, S.; Arévalo, C.; Montealegre-Melendez, I.; Muñoz, S.; Rodríguez-Ortiz, J.A.; Trueba, P.; Torres, Y. Porous Titanium for biomedical applications: Evaluation of the Conventional powder metallurgy frontier and space-holder technique. *Appl. Sci.* **2019**, *9*, 982. [CrossRef]
45. Teughels, W.; Van Assche, N.; Sliepen, I.; Quirynen, M. Effect of material characteristics and/or surface topography on biofilm development. *Clin. Oral Implants Res.* **2006**, *17*, 68–81. [CrossRef] [PubMed]
46. Le Guéhennec, L.; Soueidan, A.; Layrolle, P.; Amouriq, Y. Surface treatments of titanium dental implants for rapid osseointegration. *Dent. Mater.* **2007**, *23*, 844–854. [CrossRef] [PubMed]
47. Wennerberg, A.; Albrektsson, T. Effects of titanium surface topography on bone integration: A systematic review. *Clin. Oral Implants Res.* **2009**, *20*, 172–184. [CrossRef] [PubMed]
48. Yin, X.Z.; Xiao, T.Q.; Nagia, A.; Yang, S.; Lu, X.-L.; Shao, Q.; He, Y.; York, P.; Zhang, J.-W. In situ 3D topographic and shape analysis by synchrotron radiation X-ray microtomography for crystal form identification in polymorphic mixtures. *Sci. Rep.* **2016**, *6*, 24763. [CrossRef] [PubMed]
49. Graham, M.V.; Cady, N.C. Nano and microscale topographies for the prevention of bacterial surface fouling. *Coatings* **2014**, *4*, 37–59. [CrossRef]
50. Whitehead, K.A.; Verran, J. The effect of surface topography on the retention of microorganisms. *Food Bioprod. Process.* **2006**, *84*, 253–259. [CrossRef]
51. Nielsen, L.F. On strength of porous material: Simple systems and densified system. *Mater. Struct.* **1998**, *31*, 651–661. [CrossRef]
52. Torres, Y.; García-Ostos, C.; Arevalo, C.; Gotor, F.J.; Pavón, J.J.; Trueba, P.; Rodriguez-Ortiz, J.A. Processing and characterization of surrogate nuclear materials with controlled radial porosity. *J. Nucl. Sci. Technol.* **2017**, *54*, 167–173. [CrossRef]
53. Montero, J.F.; Tajiri, H.A.; Barra, G.M.; Fredel, M.C.; Benfatti, C.A.; Magini, R.S.; Pimienta, A.L.; Souza, J.C. Biofilm behavior on sulfonated poly (ether-ether-ketone)(sPEEK). *Mater. Sci. Eng. C* **2017**, *70*, 456–460. [CrossRef]
54. Brum, R.S.; Monich, P.R.; Fredel, M.C.; Contri, G.; Ramoa, S.D.A.S.; Magini, R.S.; Benfatti, C.A.M. Polymer coatings based on sulfonated-poly-ether-ether-ketone films for implant dentistry applications. *J. Mater. Sci. Mater. Med.* **2018**, *29*, 132. [CrossRef] [PubMed]
55. Yuan, B.; Cheng, Q.; Zhao, R.; Zhu, X.; Yang, X.; Yang, X.; Zhang, K.; Song, Y.; Zhang, X. Comparison of osteointegration property between PEKK and PEEK: Effects of surface structure and chemistry. *Biomaterials* **2018**, *170*, 116–126. [CrossRef] [PubMed]